J|A|C|S
ARTICLES

Published on Web 11/05/2009

Characterizing Dynamic Protein−Protein Interactions Using Differentially Scaled Paramagnetic Relaxation Enhancement

Dongmei Yu, Alexander N. Volkov, and Chun Tang*

Department of Biochemistry, University of Missouri, Columbia, Missouri 65211

Received August 6, 2009; E-mail: tangch@missouri.edu

Abstract: Paramagnetic relaxation enhancement (PRE) is a powerful NMR technique that allows direct visualization of minor species. The PRE is obtained by conjugating a paramagnetic probe, such as EDTA−Mn^{2+}, at a specific cysteine residue. For a fast exchange between major and minor species, the observed PRE rate approaches population-weighted average of PRE values for both states. We have employed a tripeptide of Cu^{2+}-binding paramagnetic probe that yields a much weaker PRE effect than EDTA−Mn^{2+} does. We show that by using two probes of different paramagnetic strengths attached at the same site, the relative population and exchange time scale can be extracted, providing that the dynamic event occurs in the second to millisecond regime. Hence, this improved PRE scheme, differentially scaled paramagnetic relaxation enhancement (DiSPRE), permits both temporal and spatial characterization of a dynamic system. When applying the DiSPRE scheme to reassess the weak interactions between the N-terminal domain of enzyme I and phosphocarrier protein (HPr) from the bacterial phopshotransferase system, we have identified a minor species of excited-state complex with a ∼4% population and exchanging with the stereospecific complex at ∼1100 s^{-1}. Such species is distinct from other encounter complexes previously characterized and is likely a result of promiscuity of the HPr binding interface.

Introduction

Traditionally, protein structure determination to atomic resolution has been aimed at a single static conformation that agrees with the experimental data. Such structure usually represents the most populated species associated with the lowest energy. However, transient excursions from the ground state, i.e. protein dynamics, pertain to the mechanisms of protein functions, including macromolecular association, enzymatic catalysis, and allosteric regulation.[1] Thus, characterization of protein dynamics presents a challenging yet exciting theme in biophysics and structural biology.

Solution NMR is uniquely suited to depict protein dynamics over a broad range of time scales. Relaxation dispersion is a notable NMR technique that allows identifications of residues involved in chemical exchange on a microsecond to millisecond time scale, a regime in which protein activities usually take place.[2] Relaxation dispersion works by assessing the contribution of chemical exchange (R_{ex}) toward overall apparent transverse relaxation rate (R_2). Providing that the R_{ex} contribution is large enough and by repeating the experiment at different field strengths, the relative populations (p_A and p_B) and chemical shift difference ($\Delta\omega$) can in theory be extracted for a two-state exchange.[3] Although chemical shift values depend on the protein structure, it is difficult to back-calculate the structure of minor species from chemical shifts alone. A recent tour de force has shown that the structure of minor species can be obtained by supplementing chemical shift data with residual dipolar couplings and chemical shift anisotropies of the minor species.[4]

A recent advancement in paramagnetic NMR, namely paramagnetic relaxation enhancement (PRE), has permitted *direct* visualization of minor species in rapid exchange with the ground-state main species.[5,6] With a paramagnetic probe such as EDTA−Mn^{2+} or nitroxide spin radical conjugated at a desired site, hundreds of PRE observations can be obtained simultaneously from the dipolar interaction between an unpaired electron and adjacent nuclei. The transverse relaxation enhancement rate, Γ_2, can be very large, owing to the large magnetic moment of an unpaired electron of the paramagnetic probe and r^{-6} distance dependence. The PRE is exquisitely sensitive to the minor species providing that the exchange between the major and minor species occurs in a fast exchange time scale ($k_{ex} \gg \Gamma_2$) and the paramagnetic probe is closer to the observed nuclei in the minor species. The technique has been successfully applied to investigate the dynamics of a number of systems, including protein−protein[7,8] and protein−DNA[9] complexes, protein oligomers,[10,11] natively unfolded proteins,[12,13] and

(1) Henzler-Wildman, K.; Kern, D. *Nature* **2007**, *450*, 964–972.
(2) Mittermaier, A.; Kay, L. E. *Science* **2006**, *312*, 224–228.
(3) Skrynnikov, N. R.; Dahlquist, F. W.; Kay, L. E. *J. Am. Chem. Soc.* **2002**, *124*, 12352–12360.
(4) Vallurupalli, P.; Hansen, D. F.; Kay, L. E. *Proc. Natl. Acad. Sci. U.S.A.* **2008**, *105*, 11766–11771.
(5) Clore, G. M.; Tang, C.; Iwahara, J. *Curr. Opin. Struct. Biol.* **2007**, *17*, 603–616.
(6) Clore, G. M.; Iwahara, J. *Chem. Rev.* **2009**, *109*, 4108–4139.
(7) Tang, C.; Iwahara, J.; Clore, G. M. *Nature* **2006**, *444*, 383–386.
(8) Volkov, A. N.; Worrall, J. A.; Holtzmann, E.; Ubbink, M. *Proc. Natl. Acad. Sci. U.S.A.* **2006**, *103*, 18945–18950.
(9) Iwahara, J.; Clore, G. M. *Nature* **2006**, *440*, 1227–1230.
(10) Tang, C.; Ghirlando, R.; Clore, G. M. *J. Am. Chem. Soc.* **2008**, *130*, 4048–4056.
(11) Tang, C.; Louis, J. M.; Aniana, A.; Suh, J. Y.; Clore, G. M. *Nature* **2008**, *455*, 693–696.

multidomain proteins undergoing quaternary movement.[14,15] However, if no other types of experimental inputs are available, only the lower limit of the minor species population can be determined. Moreover, the PRE values for the minor species cannot be determined if the exchange occurs on a relatively slow time scale.

Here we propose an improved PRE technique, which utilizes different paramagnetic strengths of two transition metals, Mn^{2+} and Cu^{2+}, and affords not only direct visualization of the minor species but also the associated exchange time scale and population of the minor species. During a revisit to the weak interactions between the amino-terminal domain of enzyme I (EIN) and histindine phosphocarrier protein (HPr), the first binary complex in the bacterial phosphotransferase system (PTS), we have identified a minor, excited-state species that is distinct from other encounter complexes and may be aberrantly formed as a result of the promiscuity of the HPr binding interface.

Theoretical Consideration

The transverse paramagnetic enhancement rate Γ_2 for a proton was first described by Solomon and Bloembergen[16,17] and is given by eq 1

$$\Gamma_2 = \frac{1}{15}\left(\frac{\mu_0}{4\pi}\right)^2 \gamma_I^2 g^2 \mu_B^2 S(S+1) r^{-6}\left(4\tau_c + \frac{3\tau_c}{1+\omega_H^2\tau_c^2}\right) \quad (1)$$

in which r is the distance between the paramagnetic center and the observed proton; μ_0, the permeability of vacuum; γ_I, proton gyromagnetic ratio; g, the electron g-factor; μ_B, the electron Bohr magneton; S, the electron spin quantum number; τ_c, the total correlation time defined as $(1/\tau_r + 1/\tau_e)^{-1}$, where τ_r and τ_e are the rotational correlation time and electron relaxation time, respectively; and ω_H, proton Larmor frequency. Like Mn^{2+}, Cu^{2+} has an isotropic g-tensor; hence, it exerts only line broadening but no pseudocontact shift effect on adjacent protons. The τ_e for Cu^{2+} is between 1 and 5 ns,[18] whereas the τ_e for Mn^{2+} has been experimentally determined at 9.6 ns.[19] The electron spin quantum numbers S for Cu^{2+} and Mn^{2+} are 1/2 and 5/2, respectively. Taken together, for a 40 kDa protein complex of EIN−HPr with a τ_r of 14.2 μs,[7] the ^{1}H Γ_2 rate measured on a 800 MHz spectrometer can be 18−72 times weaker for Cu^{2+} than for Mn^{2+} (Supporting Information, Figure S1). The $\Gamma_2(Mn^{2+})$ over $\Gamma_2(Cu^{2+})$ ratio drops off quickly for Cu^{2+} τ_e of 1 to 2 ns and then levels off; we found a τ_e of ~4.3 ns and a ratio of ~20 is most consistent with our experimental data.

Here we consider a two-state exchange system, between major species A and minor species B, with p_A and p_B being the associated populations and $p_A \gg p_B$. If a proton in the minor species B is closer to the paramagnetic probe than it is in the major species A, it would experience a much larger PRE effect proportional to r^{-6} ($\Gamma_{2,B} \gg \Gamma_{2,A}$). For a Mn^{2+}-based probe, at the fast exchange limit when $k_{ex} \gg [\Gamma_{2,B}(Mn^{2+}) - \Gamma_{2,A}(Mn^{2+})]$ or simply $k_{ex} \gg \Gamma_{2,B}(Mn^{2+})$, the observed PRE approaches population-weighted average of $\Gamma_{2,A}(Mn^{2+})$ and $\Gamma_{2,B}(Mn^{2+})$. $\Gamma_2^{obs}(Mn^{2+})$ at the fast exchange limit is denoted as $\Gamma_2^{\infty}(Mn^{2+})$, which is defined as

$$\Gamma_2^{\infty}(Mn^{2+}) = p_A \times \Gamma_{2,A}(Mn^{2+}) + p_B \times \Gamma_{2,B}(Mn^{2+}) \quad (2)$$

When $\Gamma_{2,A}(Mn^{2+})$ is negligible, eq 2 becomes $\Gamma_2^{\infty}(Mn^{2+}) = p_B \times \Gamma_{2,B}(Mn^{2+})$. From this equation, p_B and $\Gamma_{2,B}(Mn^{2+})$ cannot be independently determined if without additional experimental input. At a slower exchange rate, the observed PRE rate can be simulated using the McConnell equation.[9,20] As shown in Figure 1A, with an exchange rate constant k_{ex} 10 times larger than $\Gamma_{2,B}$, the Γ_2^{obs} is 90% of the population-weighted average, Γ_2^{∞}; the Γ_2^{obs} is only 50% of Γ_2^{∞} when k_{ex} is equal to $\Gamma_{2,B}$. Therefore, the fast exchange condition often cannot be satisfied for an exchange occurring on the microsecond to millisecond time scale, and it is particularly true when using a strong paramagnetic probe like EDTA−Mn^{2+}.

PREs experienced by the same proton in the minor species and originating from two different probes are denoted as $\Gamma_{2,B}(Mn^{2+})$ and $\Gamma_{2,B}(Cu^{2+})$, respectively. Because $\Gamma_{2,B}(Cu^{2+})$ is smaller than $\Gamma_{2,B}(Mn^{2+})$, at the same exchange rate, the $\Gamma_2^{obs}(Cu^{2+})$ reaches the population-weighted average, $\Gamma_2^{\infty}(Cu^{2+})$, more readily than $\Gamma_2^{obs}(Mn^{2+})$ does. As shown in Figure 1B, in the microsecond to millisecond exchange time regime, the ratio between $\Gamma_2^{obs}(Mn^{2+})$ and $\Gamma_2^{obs}(Cu^{2+})$ is always smaller than 20, the ratio between $\Gamma_2^{\infty}(Mn^{2+})$ and $\Gamma_2^{\infty}(Cu^{2+})$. The slower the conformational exchange, the smaller the ratio between the observed PRE values from the two paramagnetic probes. Such relationship can be expressed in the following equation, in which f represents a numerical solution of the McConnell equation:[20]

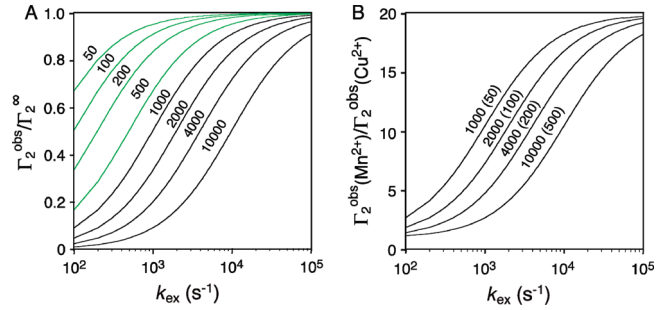

Figure 1. Dependence of the observed PRE ^{1}H Γ_2^{obs} on the exchange rate constant k_{ex}. (A) The ratio between Γ_2^{obs} and Γ_2^{∞} as a function of k_{ex} and $\Gamma_{2,B}$. In a two-state exchange between A and B, Γ_2^{∞} is defined as population-weighted average of $\Gamma_{2,A}$ and $\Gamma_{2,B}$, the PRE values for each state. With p_B of 1% and $\Gamma_{2,A}$ of 0 s^{-1}, theoretical calculations were performed for eight different values of $\Gamma_{2,B}$: 50, 100, 200, 500, 1000, 2000, 4000, and 10 000 s^{-1}. The first four $\Gamma_{2,B}$ values (green curves) are commonly afforded by a Cu^{2+}-based probe, and the last four $\Gamma_{2,B}$ values (black curves) can be caused by a Mn^{2+} probe. (B) The ratio between Γ_2^{obs} values obtained using Mn^{2+} and Cu^{2+} paramagnetic probes attached at the same site, with the Γ_2^{obs} values taken from panel A. A theoretical value of 20 for $\Gamma_2^{\infty}(Mn^{2+})$ over $\Gamma_2^{\infty}(Cu^{2+})$ ratio is used. When the k_{ex} is in the range of 10^2-10^5 s^{-1} (10 μs−10 ms), the $\Gamma_2^{obs}(Mn^{2+})$ over $\Gamma_2^{obs}(Cu^{2+})$ ratios are always smaller than 20.

(12) Mukrasch, M. D.; Bibow, S.; Korukottu, J.; Jeganathan, S.; Biernat, J.; Griesinger, C.; Mandelkow, E.; Zweckstetter, M. *PLoS Biol.* **2009**, *7*, e34.
(13) Eliezer, D. *Curr. Opin. Struct. Biol.* **2009**, *19*, 23–30.
(14) Tang, C.; Schwieters, C. D.; Clore, G. M. *Nature* **2007**, *449*, 1078–1082.
(15) Gelis, I.; Bonvin, A. M.; Keramisanou, D.; Koukaki, M.; Gouridis, G.; Karamanou, S.; Economou, A.; Kalodimos, C. G. *Cell* **2007**, *131*, 756–769.
(16) Solomon, I. *Phys. Rev.* **1955**, *99*, 559–565.
(17) Bloembergen, N. *J. Chem. Phys.* **1957**, *27*, 572–573.
(18) Banci, L.; Bertini, I.; Luchinat, C. *Magn. Reson. Rev.* **1986**, *11*, 1–40.
(19) Iwahara, J.; Schwieters, C. D.; Clore, G. M. *J. Am. Chem. Soc.* **2004**, *126*, 5879–5896.
(20) McConnell, H. M. *J. Chem. Phys.* **1958**, *28*, 430–431.

$$\begin{cases} \Gamma_2^{obs}(Mn^{2+}) = f[p_B, \Gamma_{2,B}(Mn^{2+}), k_{ex}] \\ \Gamma_2^{obs}(Cu^{2+}) = f[p_B, \Gamma_{2,B}(Cu^{2+}), k_{ex}] \\ \Gamma_{2,B}(Mn^{2+}) = 20 \times \Gamma_{2,B}(Cu^{2+}) \end{cases} \quad (3)$$

The intrinsic ^1H R_2 values can be determined from diamagnetic control; the PRE Γ_2 values for the major species, $\Gamma_{2,A}(Mn^{2+})$ and $\Gamma_{2,A}(Cu^{2+})$, can be calculated from the ground-state structure and may often be negligible. Solving this equation would afford the values of $\Gamma_{2,B}$, k_{ex} and p_B simultaneously, while a more unique solution can be obtained when more than one residue experiences the same exchange process (Supporting Information, Figure S2). We call this improved PRE scheme differentially scaled paramagnetic relaxation enhancement, or DiSPRE, which provides a temporal and spatial characterization of a dynamic system. As a proof of principle, we applied this method to characterize the transient protein−protein interactions between EIN and HPr.

Results and Discussion

Measurement of Intermolecular PRE Rates between EIN and HPr. We have designed a new scheme to introduce a Cu^{2+} paramagnetic probe. The amino-terminal Cu^{2+} (Ni^{2+}) binding (ATCUN) motif consists of three residues, Gly-Xxx-His (Xxx is any residue), and binds to Cu^{2+} with subfemtomolar affinity.[21] Customarily, the ATCUN motif is prepended to the amino-terminus of a protein,[22,23] which limits the distance information it can probe. We have designed a Gly-Cys-His tripeptide and conjugated it to HPr cysteine mutant via a disulfide bond (Figure 2). Binding of Cu^{2+} to HPr−GCH conjugate was evidenced by an appearance of an absorption peak at 528 nm[21] and the pale magenta color of the sample, indicating that conjugation does not disrupt the metal chelation of the peptide. A clear advantage of our scheme is that GCH−Cu^{2+} can be placed anywhere on the protein surface at an engineered cysteine residue, where a stronger paramagnetic probe EDTA−Mn^{2+} would also be attached.

The intermolecular PRE Γ_2 rates were obtained for EIN backbone amide protons by conjugating a paramagnetic probe at HPr. The PRE values originating from an EDTA−Mn^{2+} probe were measured as described previously.[7] In comparison, the PRE values from the GCH−Cu^{2+} probe are much weaker (Figure 3A,B). With a Cu^{2+} τ_e optimized to 4.3 ns and a Γ_2 (Mn^{2+}) over Γ_2(Cu^{2+}) ratio of 20, the Cu^{2+} PRE values for the stereospecific EIN−HPr complex, residues 52−91 at E25C, can be largely back-calculated (Figure 3B). PREs arising from minor nonspecific complexes for both E5C and E25C conjugation sites are also scaled down, mostly to the noise range, when using the GCH−Cu^{2+} probe (Figure 3A,B). The most prominent exception is a cluster of residues on EIN, residues 119−122 located at the peripheral of the protein interface, for HPr E25C conjugation site, which display an unusual scaling of PRE values, with the $\Gamma_2^{obs}(Mn^{2+})/\Gamma_2^{obs}$ (Cu^{2+}) ratio as small as 4 (Figure 3B). Several other residues such as 132 and 189 also display differentially scaled PREs. Since they are either not solvent exposed or do not form a contiguous protein surface, these residues are not included in the subsequent simulation.

The GCH peptide is a good approximation of EDTA and probes similar distance information. The randomized ensembles of GCH−Cu^{2+} and EDTA−Cu^{2+} afford similar spatial distributions, albeit that the former is more confined (Supporting Information, Figure S3A). The intermolecular PREs obtained through conjugating EDTA−Cu^{2+} probe to HPr−E25C also appear similar to that of GCH−Cu^{2+}, with the profiles for EIN residues 52−91 and residues 119−122 are essentially the same (Supporting Information, Figure S3B). However, certain regions of the protein, i.e., residues 28−39, 93−101, and 176−190, display PREs when probed by EDTA−Cu^{2+} and by EDT−Mn^{2+},[7] but not by GCH−Cu^{2+}. The reason for the differences can be 2-fold: it may be due to the different charge and shape between EDTA and GCH probes, and the distribution of minor EIN−HPr encounter complexes is somewhat perturbed in the latter; it may also be an artifact if EDTA-based probes weakly interact with EIN. Moreover, there are many conformers of EIN−HPr nonspecific encounter complexes at various occupancies and exchanging with the specific complex at different rates.[7] As a proof of principle of the DiSPRE method and to simplify the interpretation for EIN−HPr intermolecular PREs, we will use a two-state exchange model between the stereospecific complex and minor nonspecific complex that gives rise to the differentially scaled PRE values for EIN residues 119−122.

The differential scaling of intermolecular PREs were not observed for two other weak protein complexes, HPr−HPr[10] and $IIA^{Mannitol}$−HPr.[7] Cu^{2+} PREs observed for the former are mostly in the noise range, whereas PREs observed for the latter are scaled down almost uniformly from Mn^{2+} values (Supporting Information, Figure S4). Large PRE values observed for $IIA^{Mannitol}$ residues 121−127 cannot be accounted for by the specific complex and are indicative of one or more nonspecific complexes. However, the ∼20 fold scaling from Mn^{2+} to Cu^{2+} PRE values precludes determination of p_B and k_{ex} using the DiSPRE method.

Simulation of the Exchange Process for EIN−HPr Complex. To obtain a solution for eq 3, we performed a grid search varying all three parameters: p_B, k_{ex}, and $\Gamma_{2,B}$ (Cu^{2+}) (Supporting Information, Figure S2). For each combination, the differences between the observed and calculated PRE Γ_2 values for EIN residues 119−122 were calculated and the resulting PRE Q-factors were plotted (Figure 3C). Most solutions lie in a strip of $k_{ex} = 500-1500\ s^{-1}$ and $p_B = 3-10\%$, with the lowest point at $k_{ex} = 1100\ s^{-1}$ and $p_B = 4\%$ and a corresponding Q-factor of 0.06. The PRE values at the global minimum were used for structural calculations. When fit individually, the optimal k_{ex} and p_B values for residues 119, 121, and 122 are located in a similar region (Supporting Information, Figure S5). The larger spread is due to lesser stringency for an individual fit, whereas overall consistency suggests that a single minor species of EIN−HPr complex likely accounts for the differentially scaled PREs observed for EIN residues 119−122. As a control, we performed simulation for $IIA^{Mannitol}$−HPr inputted with Mn^{2+} and Cu^{2+} PRE values for residues 121, 126, and 127 (Supporting Information, Figure S4). As the ratios between the Mn^{2+} and Cu^{2+} PREs are close to the theoretical value, simulation did not yield converged p_B and k_{ex} values (Supporting Information, Figure S6).

At a rate constant of 1100 s^{-1}, the exchange time scale between major specific and minor nonspecific EIN−HPr

(21) Lau, S. J.; Kruck, T. P.; Sarkar, B. *J. Biol. Chem.* **1974**, *249*, 5878–5884.
(22) Donaldson, L. W.; Skrynnikov, N. R.; Choy, W. Y.; Muhandiram, D. R.; Sarkar, B.; Forman-Kay, J. D.; Kay, L. E. *J. Am. Chem. Soc.* **2001**, *123*, 9843–9847.
(23) Mal, T. K.; Ikura, M.; Kay, L. E. *J. Am. Chem. Soc.* **2002**, *124*, 14002–14003.
(24) Garrett, D. S.; Seok, Y. J.; Peterkofsky, A.; Gronenborn, A. M.; Clore, G. M. *Nat. Struct. Biol.* **1999**, *6*, 166–173.

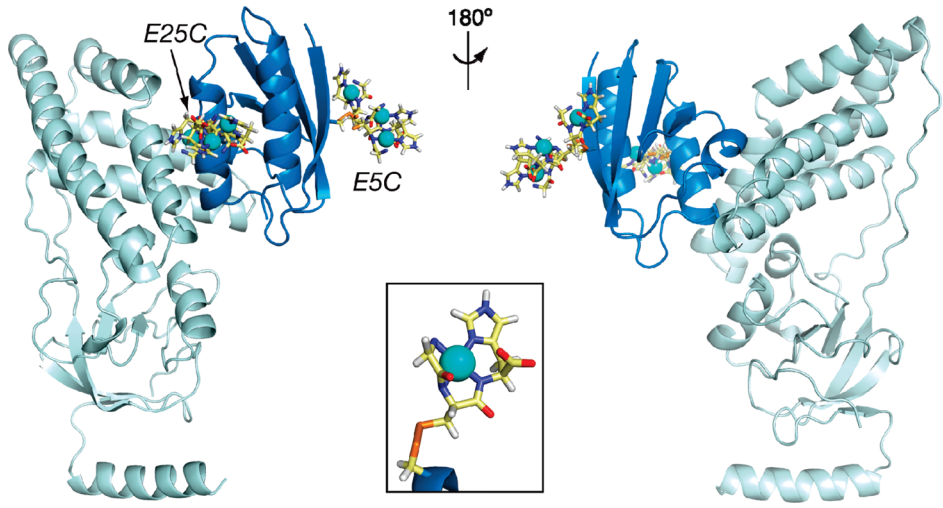

Figure 2. Structure of the stereospecific complex between EIN and HPr. The coordinates are taken from PDB entry 3EZA[24] and are shown in two different views. EIN is colored in light blue and HPr in dark blue. The GCH peptide conjugated at either E5C or E25C of HPr is shown as sticks, with the bound Cu^{2+} shown as a blue sphere, and other atoms are color-coded by the element. The torsion angles for the linker between GCH peptide and HPr are randomized and a three-conformer representation of GCH−Cu^{2+} is shown. The inset shows GCH−Cu^{2+} coordination geometry and the covalent protein−peptide disulfide bond at HPr E25C.

complexes is much slower than the rate expected for the formation of an encounter complex.[25] The rapid formation of encounter complexes facilitates protein−protein association and formation of the final stereospecific complex. Using the PRE technique, the encounter complexes between EIN and HPr have been previously experimentally visualized.[7] The population for each member of the encounter complexes would be extremely small, while collectively these complexes form a molecular cloud shaped by the electrostatic potential. On the other hand, the lower limit of EIN−HPr dissociation rate constant was 1100 s^{-1}, estimated from chemical shift perturbation.[26] Therefore, with a p_B of ∼4% (corresponding to ∼2 kcal/mol free energy difference from the ground state) and a k_{ex} of 1100 s^{-1}, the minor species of EIN−HPr complex is possibly a kinetically trapped species and represents an excited-state conformer, distinguishing itself from other encounter complexes.

Comparison to Relaxation Dispersion. To assess if the presence of minor excited-state EIN−HPr complex contributes to backbone ^{15}N transverse relaxation rates, we performed CPMG relaxation dispersion experiment.[27] Most residues display no change in ^{15}N R_2 relaxation rates at increasing ^{15}N 180° pulsing rate, except for a few interfacial residues, including Thr34 and Leu50 of HPr, whose relaxation dispersion profiles can be tentatively fit with k_{ex} values of 4948 ± 2754 and 3558 ± 1280 s^{-1}, respectively (Supporting Information, Figure S7). Relaxation dispersion characterization of protein complexes has been previously demonstrated on GB1 mutant dimer[28] and $IIA^{Mannitol}$−$IIB^{Mannitol}$.[29] The exchange rate for GB1 dimer is on the order of 10^2 s^{-1}, while IIA/$IIB^{Mannitol}$ is on the order of 10^4 s^{-1}. Although at a similar K_D to EIN−HPr complex, GB1 dimerization is coupled with partial unfolding, whereas $IIA^{Mannitol}$ and $IIB^{Mannitol}$ interact with each other at millimolar K_D. Therefore, our determined k_{ex} value fits nicely into the series. Thr34 and Leu50 of HPr experience the largest chemical shift perturbation upon binding to EIN, with $\Delta\omega$ of 0.725 and 0.856 ppm, respectively.[26] Using these $\Delta\omega$ values, the populations of minor unbound species can be determined at 9.3 ± 4.3% and 22.4 ± 17.9%, corresponding to K_D values in the range of 1−10 and 1−100 μM, respectively. The values obtained from two individual fits are consistent with each other and are also consistent with the K_D value of 3.7 ± 0.3 μM previously determined using isothermal calorimetry.[30] Taken together, relaxation dispersion revealed the exchange between free protein and bound specific complex.

Since there is no indication that the minor excited-state EIN−HPr complex contributes to ^{15}N relaxation rates, the chemical shift differences $\Delta\omega$ between specific complex and nonspecific complex are likely very small. Therefore, the assumption of identical chemical shifts is justified when simulating the McConnell equation (Supporting Information, Figure S2). For other exchanging systems in which the chemical shift differences between the two states are sufficiently large, it is possible to solve the relaxation dispersion equation[27,31] in conjunction with eq 3, which would afford a more unambiguous solution of minor species p_B and exchange rate k_{ex}. As such, the DiSPRE method offers complementary information to the relaxation dispersion technique.

Structural Model of the Excited-State EIN−HPr Complex. Refined against $\Gamma_{2,B}(Cu^{2+})$ PRE restraints and supplemented by radius-of-gyration and database restraints, we have obtained a structural model for the minor, excited-state EIN−HPr complex (Figure 4A). The conformers obtained with $\Gamma_{2,B}(Mn^{2+})$ restraints are similar to those calculated with $\Gamma_{2,B}(Cu^{2+})$ (Supporting Information, Figure S8). Using a combination of 96% stereospecific complex and 4% minor species at an exchange rate constant of 1100 s^{-1}, the back-calculated PREs are in good agreement

(25) Gabdoulline, R. R.; Wade, R. C. *Curr. Opin. Struct. Biol.* **2002**, *12*, 204–213.
(26) Garrett, D. S.; Seok, Y. J.; Peterkofsky, A.; Clore, G. M.; Gronenborn, A. M. *Biochemistry* **1997**, *36*, 4393–4398.
(27) Tollinger, M.; Skrynnikov, N. R.; Mulder, F. A.; Forman-Kay, J. D.; Kay, L. E. *J. Am. Chem. Soc.* **2001**, *123*, 11341–11352.
(28) Jee, J.; Ishima, R.; Gronenborn, A. M. *J. Phys. Chem. B* **2008**, *112*, 6008–6012.
(29) Suh, J. Y.; Iwahara, J.; Clore, G. M. *Proc. Natl. Acad. Sci. U.S.A.* **2007**, *104*, 3153–3158.
(30) Suh, J. Y.; Tang, C.; Clore, G. M. *J. Am. Chem. Soc.* **2007**, *129*, 12954–12955.
(31) Mulder, F. A.; Mittermaier, A.; Hon, B.; Dahlquist, F. W.; Kay, L. E. *Nat. Struct. Biol.* **2001**, *8*, 932–935.

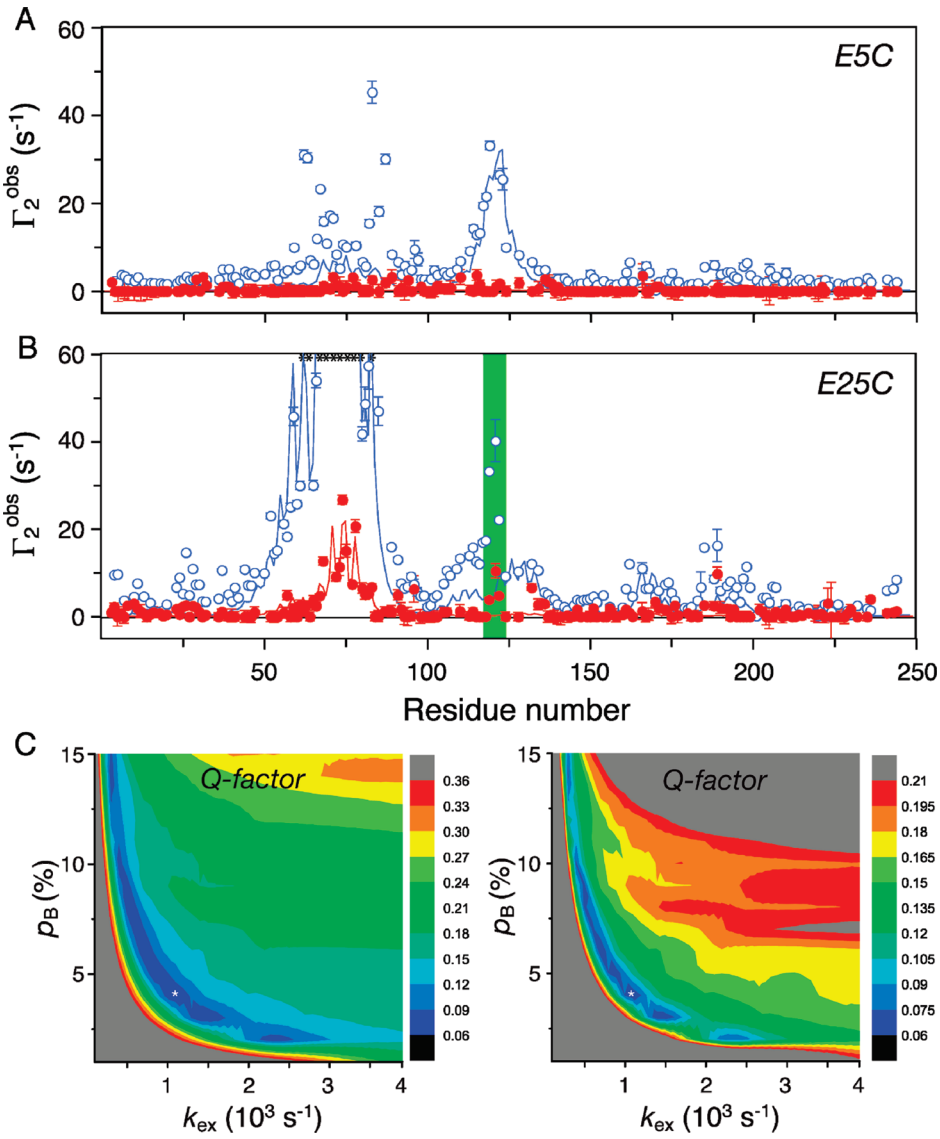

Figure 3. Observed and simulated intermolecular PRE Γ_2 rates. (A, B) PRE profiles of EIN in complex with EDTA−Mn^{2+} (blue open circles) or GCH−Cu^{2+} (red filled circles) conjugated at E5C and E25C of HPr. Error bars represent one standard deviation. Asterisks indicate EIN residues that are broadened out in the EDTA−Mn^{2+} sample. The solid lines show PRE values for EDTA−Mn^{2+} (blue) or GCH−Cu^{2+} (black) calculated for the stereospecific EIN−HPr complex by optimizing the ensemble conformation of the paramagnetic probe. EIN residues 119−122 that experience differentially scaled PRE effects are highlighted with a green box. The peak for EIN residue 120 overlaps with other peaks, precluding accurate PRE measurement. (C) Grid search for the optimal k_{ex} and p_B values that yields the differentially scaled Mn^{2+} and Cu^{2+} PRE values for residues 119, 121, and 122. The two panels are plotted with different Q-factor cutoffs and binnings. The best fit can be found in a strip of k_{ex} = 500−1500 s^{-1} and p_B = 3−10%. The global minimum at k_{ex} = 1100 s^{-1} and p_B = 4% is indicated by an asterisk.

with the observed values: the intermolecular PRE values for EIN residues 119−122 probed by both EDTA−Mn^{2+} and GCH−Cu^{2+} can be essentially reproduced (Figure 4B).

The minor, excited-state EIN−HPr complex is distinct from other encounter complexes previously visualized.[7] If excluding the EDTA−Mn^{2+} PRE restraints for residues 119, 121, and 122 at HPr E25C site, the structure ensemble calculated for the encounter complexes remain largely the same (Supporting Information, Figure S9). The HPr in the minor, excited-state complex binds close to the specific interface but adopts an opposite orientation (Figure 4A). With an area of 566 ± 242 Å^2, the buried solvent-accessible interface in the excited-state complex is smaller than that of the stereospecific complex (1948 Å^2) but larger than those in the encounter complexes (241 ± 177 Å^2). Therefore, to overcome stabilizing interactions across a relatively broad interface and to perform a large movement may account for the slow interconversion between the two EIN−HPr complexes. Indeed, in a previous physics-based docking model of EIN−HPr complex guided by intermolecular PREs, a significant population of nonspecific complexes is found near the specific interface with alternative orientations.[32] The relationship among free proteins and three types of EIN−HPr complexes is illustrated in Figure 5.

The nonspecific excited-state complex formed between EIN and HPr is likely a result of the promiscuity of the HPr interface. To propagate signals within the PTS, HPr interacts with five different proteins—EIN, $IIA^{Glucose}$, $IIA^{Mannitol}$, $IIA^{Mannose}$, and $IIA^{Chitobiose}$—all utilizing similar interfaces around its active site, histidine 15. As a result, the binding specificity may be compromised. Similarly, it has been shown that the $IIA^{Mannose}$ and $IIB^{Mannose}$, two other PTS member enzymes, can form both

(32) Kim, Y. C.; Tang, C.; Clore, G. M.; Hummer, G. *Proc. Natl. Acad. Sci. U.S.A.* **2008**, *105*, 12855–12860.

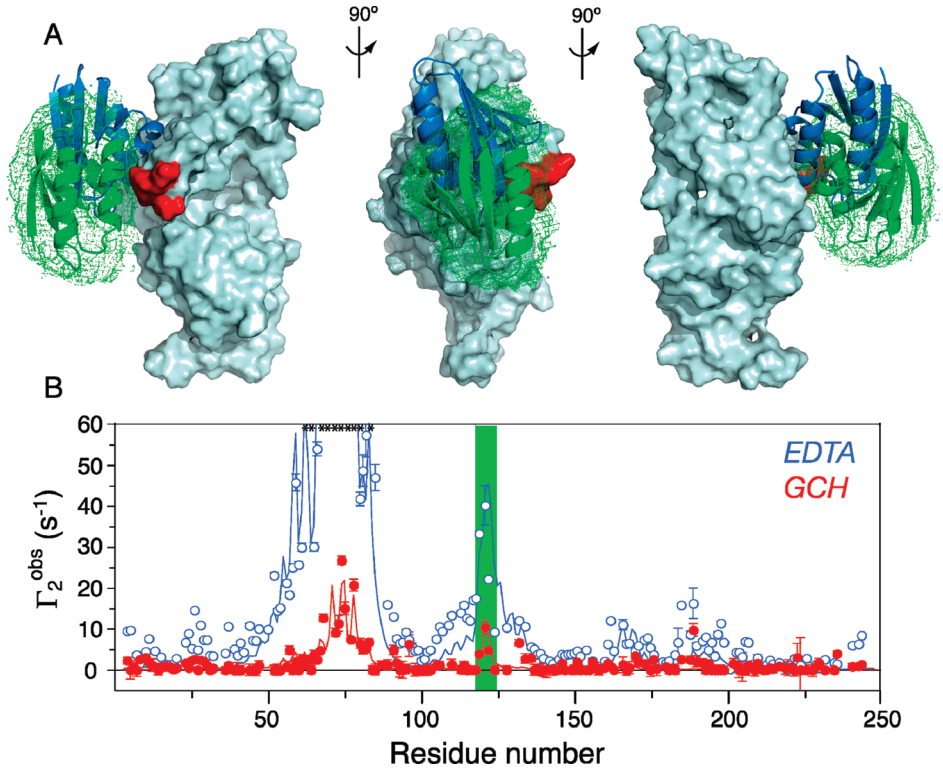

Figure 4. Structural model of the minor EIN−HPr complex with a population of 4%. (A) Three orthogonal views of the minor, excited-state EIN−HPr complex. With EIN superimposed, the atomic probability of HPr calculated for 50 lowest-energy conformers is plotted at 20% threshold and shown as green meshes. The EIN is shown as a light blue surface, HPr in the stereospecific complex is shown as a blue cartoon, the HPr conformer closest to the mean is shown as a green cartoon. EIN residues 119−122 that experience differentially scaled PRE values are colored in red. (B) Observed and calculated PRE profiles for E25C conjugation site with EDTA−Mn^{2+} and GCH−Cu^{2+} probes. The calculated values are reproduced from 96% stereospecific complex and 4% minor excited-state complex undergoing a chemical exchange with a rate constant of 1100 s^{-1}. The same color scheme is used as in Figure 3. Error bars represent one standard deviation. Note that if not for differential scaling of PRE, the observed ^1H Γ_2 values for EIN residues 121 and 122 would be greater than 200 s^{-1} when probed by EDTA−Mn^{2+}.

productive and nonproductive complexes of approximately equal occupancy, with the active site histidine correctly positioned in the former; a single point mutation at the interface of $IIA^{Mannose}$ effectively abolished the formation of nonproductive complex.[33] For other instances, the minor excited-state complexes may be favored at high protein concentrations or upon mutations or post-translational modifications.[34,35]

Concluding Remarks. Utilizing an improved PRE scheme, DiSPRE, we have characterized a conformational fluctuation between the major and minor protein complexes. We were able to simultaneously obtain minor species population, exchange time scale, and a structural model of the minor species. We envision that a third paramagnetic probe, such as maleimide−TEMPO spin radical,[14] can be introduced at the same site, which along with GCH−Cu^{2+} and EDTA−Mn^{2+} would yield a nice series of differentially scaled PREs and afford a more accurately defined exchange process (Supporting Information, Figure S10). In conclusion, the new DiSPRE scheme provides both temporal and spatial information of protein conformational fluctuations and is a valuable addition to the toolkit for characterizing macromolecular dynamics.

Materials and Methods

Sample Preparation. EIN and HPr were overexpressed in *Escherichia coli* and purified on cation exchange and size exclusion columns as previously described.[7] All buffers were treated with Chelex (Bio-Rad) to remove any metal contaminants. Cysteine mutations on HPr E5C and E25C were introduced using QuikChange (Stratagene). The GCH peptide was purchased from GenScript at 95% purity. The HPr cysteine mutants were conjugated with GCH peptide via a disulfide exchange reaction using a procedure described by Su et al.[36] Briefly, HPr was first activated by 5,5′-dithiobis(2-nitrobenzoic acid) (DTNB, Pierce) to form an HPr−TNB adduct. After removing the excess DTNB and released TNB, HPr−TNB was reacted with GCH peptide to yield an HPr−GCH adduct. $CuCl_2$ was then loaded, resulting in a pale magenta sample. The GCH attachment was verified by mass spectrometry (calculated with no bound Cu^{2+} 9406.7 Da, observed 9407.6 Da), and the extent of conjugation and metal chelation was confirmed by measuring the absorption at 528 nm (extinction coefficient 103 M^{-1} cm^{-1}).[21]

NMR Spectroscopy. The protein complex samples were prepared in 10 mM Tris HCl pH 7.5 and contained 0.3 mM each of U-[^2H,^{15}N]EIN and unlabeled HPr. HPr was either wild-type (diamagnetic control) or a cysteine mutant conjugated with a paramagnetic probe. Intermolecular PREs were collected at 310 K

(33) Hu, J.; Hu, K.; Williams, D. C., Jr.; Komlosh, M. E.; Cai, M.; Clore, G. M. *J. Biol. Chem.* **2008**, *283*, 11024–11037.
(34) Pawson, T.; Nash, P. *Science* **2003**, *300*, 445–452.
(35) Vavouri, T.; Semple, J. I.; Garcia-Verdugo, R.; Lehner, B. *Cell* **2009**, *138*, 198–208.
(36) Su, X. C.; Huber, T.; Dixon, N. E.; Otting, G. *ChemBioChem* **2006**, *7*, 1599–1604.

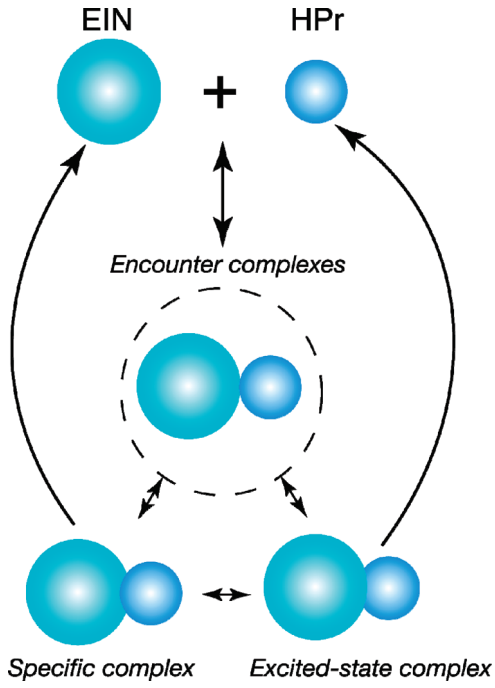

Figure 5. Schematic representation for the relationship among free EIN and HPr proteins and their encounter complexes, stereospecific complex, and minor excited-stated complex. To facilitate the formation of final specific complex, EIN and HPr first form a cloud of electrostatically steered encounter complexes.[7] The minor excited-state complex has a population of ~4%, and it only becomes a productive, specific complex by reorienting itself around the interface at an exchange rate of 1100 s^{-1}. All three types of complexes may dissociate back to free proteins.

on a Bruker Avance III Ultrashield 800 MHz spectrometer equipped with a cryogenic TCI probe. A two time-point, $^{1}H-^{15}N$ correlation experiment was used to measure backbone amide PRE as previously described.[19,37] The CPMG relaxation dispersion experiment[27] was applied to the 0.3 mM complex of ^{15}N-HPr and unlabeled EIN complex. The effective field strengths used are 41.9, 84.5, 127.6, 171.2, 215.5, 260.4, 352.1, 446.4, 543.5, 746.3, 961.5, and 1250 Hz.

PRE Calculation and Simulation. The GCH−Cu^{2+} paramagnetic probe was represented with three conformers to account for linker flexibility.[19] The coordinates of GCH−Cu^{2+} were taken from ref 38, and the peptide moiety was treated as a rigid body. The side chain torsion angles of the linker between HPr and GCH−Cu^{2+} were randomized and optimized using Xplor-NIH.[39]

Effect of exchange on Γ_2^{obs} was simulated using line-shape analysis based on the McConnell equation[20] as described before.[19] A two-state exchange between the stereospecific EIN−HPr complex and a minor species with identical chemical shifts was assumed. The PRE values for the major species $\Gamma_{2,A}$ were calculated from the stereospecific complex of EIN−HPr,[24] upon optimizing the three-conformer representation of EDTA−Mn^{2+} or GCH−Cu^{2+}.

Simulations were performed for EIN residues 119, 121, and 122, which experience differentially scaled PRE effects. NMR resonance for EIN residue 120 overlaps with other peaks, precluding accurate PRE measurement. A grid search was performed by varying the values of $\Gamma_{2,B}(Cu^{2+})$ from 10 to 500 s^{-1} in increments of 10 s^{-1}, k_{ex} from 100 to 10 000 s^{-1} in 100 s^{-1} steps, and p_B from 0.01 to 0.2 with 0.01 per step. Proportionally, the $\Gamma_{2,B}(Mn^{2+})$ was incremented from 200 to 10 000 s^{-1} in 200 s^{-1} steps. For each $[\Gamma_{2,B}(Cu^{2+}), k_{ex}, p_B]$ combination, the expected $\Gamma_2^{calc}(Cu^{2+})$ and $\Gamma_2^{calc}(Mn^{2+})$ values were calculated. The agreement between Γ_2^{obs} and Γ_2^{calc} was assessed by PRE Q-factors defined as

$$Q = \left\{ \sum_m \sum_i [\Gamma_2^{obs}(i) - \Gamma_2^{calc}(i)]^2 / \sum_m \sum_i [\Gamma_2^{obs}(i)]^2 \right\}^{1/2} \quad (4)$$

in which i is the residue number and m stands for two different paramagnetic metals. A detailed simulation protocol is described in Supporting Information, Figure S2.

Structure Calculations. Starting from randomized relative positions and orientations, the structure of excited-state EIN−HPr complex was calculated with Xplor-NIH[39] using a restrained rigid-body simulated annealing protocol refined against the PRE and radius-of-gyration restraints.[40,41] The paramagnetic group was represented as a three-conformer ensemble and was grouped together with HPr as a rigid body. The PRE target values for residues 119, 121, and 121 from GCH−Cu^{2+} paramagnetic probe at the E25C site were 130, 350, and 40 s^{-1}, respectively, which were obtained from a global fitting of PRE values for all three residues. The structures were first calculated by treating both HPr and EIN as rigid bodies. In a second round of simulated annealing, the side chains were loosened to improve packing at the protein interface[42] and were refined in the presence of a database potential.[43] The atomic probabilities were calculated as described.[44] The structures were rendered using PyMOL.[45]

Acknowledgment. We thank Junji Iwahara for providing the script of PRE analysis and fitting routines and G. Marius Clore for helpful suggestions. The computations were performed on the HPC resources at the University of Missouri Bioinformatics Consortium. The work was supported by a startup fund from the University of Missouri.

Supporting Information Available: Additional data and calculations including a plot of dependence of theoretical $\Gamma_2(Mn^{2+})$ over Γ_2 (Cu^{2+}) ratio on Cu^{2+} relaxation correlation time τ_e; a flowchart of grid search protocol to identify optimal combination of k_{ex}, p_B, and PRE values for the minor species; comparison between EDTA−Cu^{2+} and GCH−Cu^{2+} paramagnetic probes; intermolecular PRE profiles between $IIA^{Mannitol}$ and HPr, and between HPr and HPr; grid search of PRE Q-factors for individual residues; individual and global fittings for $IIA^{Mannitol}$ residues; CPMG relaxation dispersion curves for HPr residues in the HPr−EIN complex; comparison of minor, excited-state EIN−HPr complex structures calculated with GCH−Cu^{2+} or EDTA−Mn^{2+} PRE restraints; comparison of the ensemble structure of EIN−HPr encounter complexes calculated with full set or with a subset of EDTA−Mn^{2+} restraints and an illustration of using maleimide-TEMPO as a third differential PRE probe. This material is available free of charge via the Internet at http://pubs.acs.org.

JA906673C

(37) Iwahara, J.; Tang, C.; Clore, G. M. *J. Magn. Reson.* **2007**, *184*, 185–195.
(38) Camerman, N.; Camerman, A.; Sarkar, B. *Can. J. Chem.* **1976**, *54*, 1309–1316.
(39) Schwieters, C. D.; Kuszewski, J. J.; Tjandra, N.; Clore, G. M. *J. Magn. Reson.* **2003**, *160*, 65–73.
(40) Kuszewski, J.; Gronenborn, A. M.; Clore, G. M. *J. Am. Chem. Soc.* **1999**, *121*, 2337–2338.
(41) Tang, C.; Clore, G. M. *J. Biomol. NMR* **2006**, *36*, 37–44.
(42) Clore, G. M.; Schwieters, C. D. *J. Am. Chem. Soc.* **2003**, *125*, 2902–2912.
(43) Kuszewski, J.; Gronenborn, A. M.; Clore, G. M. *Protein Sci.* **1996**, *5*, 1067–1080.
(44) Schwieters, C. D.; Clore, G. M. *J. Biomol. NMR* **2002**, *23*, 221–225.
(45) Delano, W. L. *PyMOL*; DeLano Scientific: Palo Alto, CA, 2002.